Photoproton Cross Sections of Carbon*

S. PENNER AND J. E. LEISS
National Bureau of Standards, Washington, D. C.
(Received December 31, 1958)

The partial (γ,p) cross section of carbon in which the residual boron nucleus is left in the ground state has been measured with a thin-crystal proton spectrometer. This cross section is shown to decrease from about 10 mb at the giant resonance peak (22 Mev) to about 0.1 mb near 60-Mev photon energy. Angular distributions measured at five energies exhibit an asymmetry around 90° which increases rapidly with increasing energy. The partial cross section to the first excited state of boron is $(7\pm16)\%$ of the ground-state cross section. The partial cross section to one or more excited states of boron about 5 Mev above the ground state is comparable with the ground-state cross section above 30-Mev photon energy. In addition to the cross-section data, the measurements provide a sensitive means of calibrating the energy scales of electron accelerators at energies in the 25- to 50-Mev region.

INTRODUCTION

PHOTONUCLEAR cross sections for a specific photon energy are difficult to measure because the measurements must usually be made with the continuous bremsstrahlung spectrum. For this reason, and also because highly selective experimental conditions are not generally used, most photonuclear experiments measure average properties of the photonuclear effect. For example, photoneutron cross sections measured either with a total neutron counter or by counting radioactive residual nuclei are total cross-section measurements, summed over the excited states of the residual nucleus. Indeed, if a total neutron counter is used, only the sum $(\gamma,n)+2(\gamma,2n)+(\gamma,np)$, $+\cdots$ is measured. A great deal of useful information has been obtained from this type of experiment, and considerable success has been achieved in explaining the results on the basis of statistical models. However, for light nuclei the statistical model should fail, and we expect the shell model to give more accurate descriptions. Since the low-lying excited states of light nuclei are well separated in energy, it is possible to measure partial cross sections for (γ,p) reactions which leave the residual nucleus in a particular state, by using a proton detector of reasonable energy resolution. These partial cross sections should be calculable using the shell model.

In this experiment the reaction $C^{12}(\gamma,p)B^{11}$ has been studied in the energy range above the giant resonance peak. The technique used a CsI thin-crystal spectrometer which, with careful control of the bremsstrahlung energy, allowed the measurement of the partial cross section for producing a proton and leaving the residual B^{11} nucleus in its ground state. This partial cross section has been measured as a function of angle and energy in the ranges 30° to 150° and 22 Mev to 58 Mev photon energy.

A preliminary experiment has been reported previously.[1] The present results are more reliable and extensive. Agreement with the preliminary results is satisfactory.

EXPERIMENTAL METHOD

The experimental arrangement is shown in Fig. 1. The bremsstrahlung beam from the National Bureau of Standards synchrotron, collimated to 2.5-inch diameter, strikes a thin polyethylene or polystyrene target. The target and detector are placed in vacuum to eliminate background due to photoprotons produced in air and to reduce proton energy loss so that the lowest energy protons can reach the detector.

The detector consists of a 0.0064-inch thick by $1\frac{1}{2}$-inch diameter CsI crystal mounted on a Lucite light pipe connected to an RCA 6199 photomultiplier. A thick 1.25-inch diameter brass collimator is placed in front of the crystal to reduce edge effects. The crystal and light pipe are covered with aluminum foil.

A very thin crystal was chosen to reduce background from electrons. For a thick crystal the pulse heights from electrons and protons of a few Mev are comparable. When the crystal is very thin, the electrons go through the crystal without losing much energy. Thus, for thicknesses below about 0.010 inch, the electron pulses are much smaller than the proton pulses of interest. This fact allows operation of the proton detector in a very high electron flux with practically no background.

The light pipe forms a vacuum seal at the front of the can containing the photomultiplier. Thus, the phototube is in an air environment, eliminating the

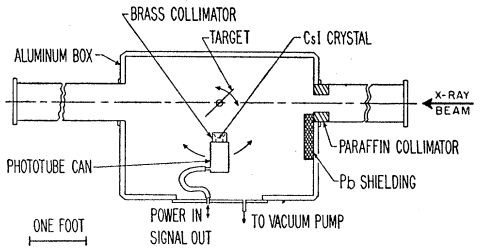

FIG. 1. Plan view of experimental arrangement.

* This project was supported by the U. S. Atomic Energy Commission.

[1] S. Penner and J. E. Leiss, Bull. Am. Phys. Soc. Ser. II, 3, 56 (1958).

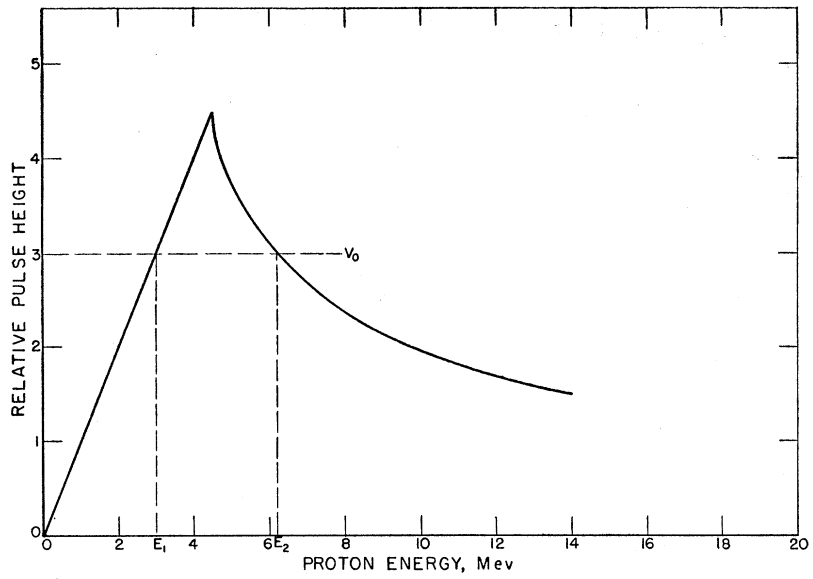

FIG. 2. Relative pulse height as a function of the energy of a proton incident on the CsI crystal. The range in g/cm² *versus* energy for CsI is assumed equal to that for silver. Pulse heights greater than V_0 are due to protons in the energy range E_1 to E_2.

problems of operating high-voltage systems in vacuum. High voltage and signal leads from the phototube come out of the vacuum system in a flexible air tight hose. The signal is fed to a cathode follower which drives the linear amplifier of an RCL 256-channel analyzer. The amplifier output goes to a linear gate circuit. The pulses are passed through the linear gate if they are large enough, and then go to the analyzer for pulse-height analysis. The linear gate is needed to remove from the spectrum the very large number of small pulses caused by electrons striking the detector, which would otherwise jam the analyzer causing a large loss of good counts.

If a proton has enough energy to pass through the crystal, the pulse height is a decreasing function of energy because of the decrease of the rate of energy loss. Figure 2 shows the pulse-height output as a function of the energy of the proton incident on the crystal. It is seen that all pulses above a preselected level V_0 are due to protons in the energy bin E_1 to E_2. If an absorber is placed between the incident protons and the detector, the energy bin determined by V_0 is shifted to higher energies. In practice the energy bin is determined by the target thickness, the amount of aluminum absorber placed in front of the detector, the pulse-height-energy relation (Fig. 2), and the pulse-height resolution of the detector. If all pulses larger than V_0 are counted, the efficiency $\eta(E)$ for detecting a proton of energy E is just the average over x of the probability that a proton of this energy originating at depth x in the target and heading toward the detector, produces a pulse height greater than V_0 in the detector. For angular distribution measurements the angle between the detector and the plane of the target is kept constant at 45°. This means that the target thickness seen by the detector is always the same, so the efficiency η is very nearly independent of the detector angle.

The resolution of the detector is about 10% of the energy lost in the crystal and is thus usually almost negligible in determining the efficiency since most of the initial proton energy is lost in the absorbers. The resolution was measured with an alpha particle source and was assumed to be the same (in terms of percent resolution) for protons because a series of tests showed that the main contribution to the resolution was nonuniformity of light collection from different parts of the crystal. We estimate that errors in the efficiency due to imperfect knowledge of the energy resolution are less than one percent. The other factors entering into the efficiency are based on the range-energy relations for protons, which are very well known.[2] Uncertainties in the measured cross sections due to errors in the efficiency are believed less than 3%. Efficiency curves calculated for each of the ten absorbers used in the experiment are shown in Fig. 3. Table I gives the target and absorber thicknesses used.

TABLE I. List of absorber and target thicknesses.

Absorber number	Absorber (mg/cm² aluminum)	Target
0	2.6[a]	24.04 mg/cm² polystyrene
1	68.9	24.04 mg/cm² polystyrene
2	134.9	47.19 mg/cm² polystyrene
3	201.2	47.19 mg/cm² polystyrene
4	268.1	68.98 mg/cm² polystyrene
7	465.7	135.4 mg/cm² polyethylene
11	731.5	135.4 mg/cm² polyethylene
15	993.2	135.4 mg/cm² polyethylene
20	1324	135.4 mg/cm² polyethylene
25	1658	135.4 mg/cm² polyethylene

[a] This is the thickness of the aluminum foil covering the face of the CsI crystal.

[2] We use the range-energy data given by W. A. Aron, University of California Radiation Laboratory Report UCRL-1325 (unpublished).

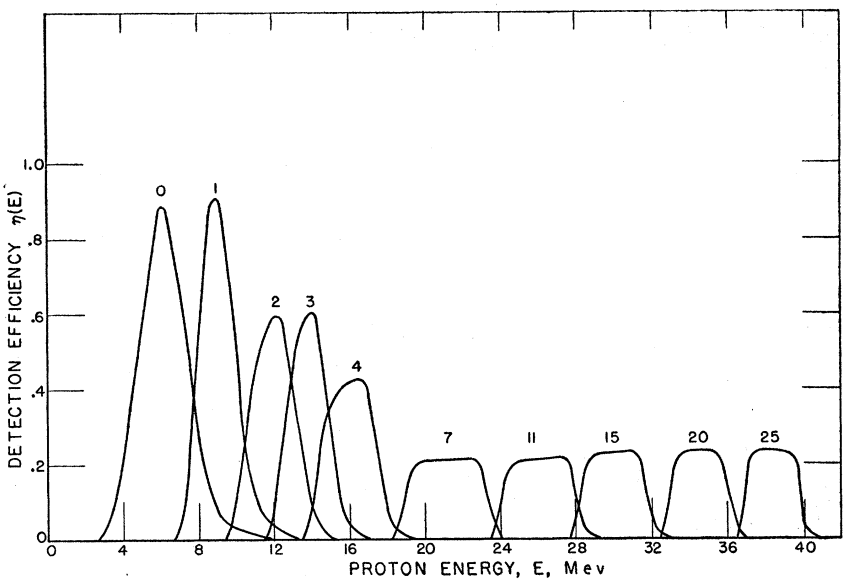

FIG. 3. Proton detection efficiency $\eta(E)$. The curves are labelled with the appropriate absorber numbers. The major contribution to the width of the curve is due to the target thickness. The sudden changes in efficiency between adjacent curves are due to changes in target thickness. Target and absorber thicknesses are given in Table I.

To measure angular distributions, the target and detector are rotated together about a point centered in the x-ray beam. Angles are set to an accuracy of better than $\pm\frac{1}{2}°$. Because of the large size of the target and detector, the angular resolution of the system is about 15° full width at half-maximum. Results are corrected for the finite angular resolution.

The detection system is calibrated with a RaD alpha-particle source to determine the pulse-height level V_0. The ratio of alpha-particle pulse height to proton pulse height at the same energy is taken to be 0.59.[3] A calibration was taken at the beginning and end of each day's runs. Drifts of about one percent over a day were observed. The calibration was checked by comparing the observed proton spectrum with a calculated spectrum based on the observed cross section and detector resolution. The comparison is shown in Fig. 4. It should be noted that the shape of the spectrum at large pulse heights is very sensitive to the energy resolution of the detector while the cross-section measurements are not. The spectrum tip shape is also much more sensitive to the calibration of the detection system than is the cross section. The agreement of the observed and calculated curves of Fig. 4 is good. An uncertainty in the cross section of less than 5% is indicated.

Because of the strong discrimination of the detector against electrons, no background was observed except at x-ray energies above 50 Mev. Even then, the background was negligible except when cross sections below 0.02 mb/sterad were observed. This background was shown to be caused by the pileup of many electron pulses occurring at nearly the same time. At forward angles, where the electron flux was highest, it was sometimes necessary to reduce the x-ray intensity to eliminate the background.

[3] Bashkin, Carlson, Douglas, and Jacobs, Phys. Rev. **109**, 434 (1958).

For all of the work presented in this report, the synchrotron was operated with a 200-μsec x-ray yield pulse which terminated at the peak of the magnetic field. The x-ray pulse length is controlled by slowly turning off the voltage on the rf cavity and letting the electrons drift into an internal target. At these low energies there is not sufficient radiation loss to allow the x-ray burst to extend past the peak of the magnetic field. The total energy spread of the x-ray burst for

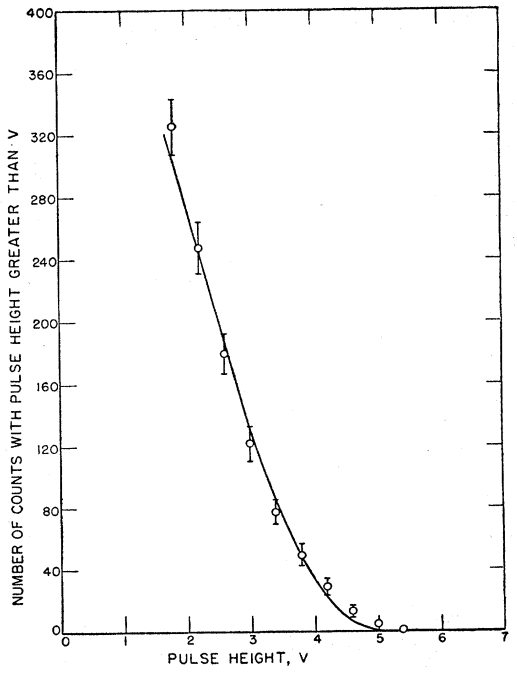

FIG. 4. Integrated pulse-height spectrum. Data taken at .06 with absorber number seven. The solid curve is the calculated proton pulse-height spectrum.

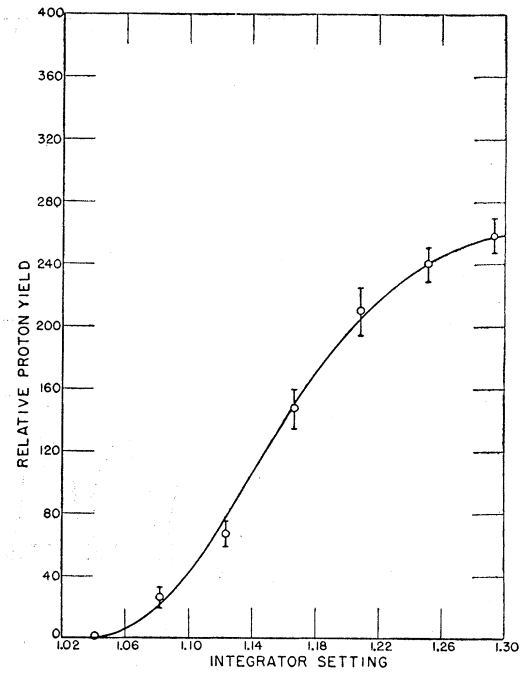

FIG. 5. Proton yield at 90° as a function of integrator setting. (a) Data taken with absorber number one. (b) Data taken with absorber number seven. The solid curves are the best-fit calculated yields assuming ground-state cross section only.

these conditions is about 1%. The stability of the synchrotron operation was about 0.2%.

The x-ray beam was monitored by a thick-walled aluminum ionization chamber which had been previously calibrated in this laboratory.[4,5] The calibration of this monitor is believed accurate to at least 3%.

ENERGY CALIBRATION

The present experiment began as an attempt to calibrate the synchrotron energy scale. The object was to obtain a relation between the setting of an integrator circuit and the corresponding peak bremsstrahlung energy in the region above 25 Mev where the usual method of calibrating energy by reaction thresholds cannot be used. We attempted to measure the threshold for detecting protons of a particular energy from the $C^{12}(\gamma,p)B^{11}$ reaction. In order to define the corresponding photon energy, it is necessary to assume that part of the time the B^{11} nucleus will be left in its ground state.

Yield curves of proton counting rate as a function of integrator setting are shown in Fig. 5 for data taken at 90° with absorbers number 1 and 7. The data in Fig. 5 define a threshold very precisely if the shape of the yield curve is known. The yield curve as a function of energy is given by

$$Y(k_0)=C\int_0^{k_0}\sigma(k)\eta(E)N(k_0,k)dk. \qquad (1)$$

In this equation $Y(k_0)$ is the yield in protons per unit x-ray yield at peak energy k_0; C is a constant depending on the target thickness and the detector solid angle; $\sigma(k)$ is the (γ,p) partial cross section to the ground state of B^{11}; $\eta(E)$ is the efficiency function previously discussed; $N(k_0,k)$ is the normalized bremsstrahlung spectrum. In the present analysis we use the Schiff integrated-over-angles spectrum as tabulated by Penfold and Leiss.[6] The relation between the proton energy E and the photon energy k was calculated using relativistic two-body dynamics and a threshold energy for the ground-state transition of 15.95 Mev.

If we assume that $\sigma(k)$ is a constant over the range in which $\eta(E)$ is not zero, we can explicitly evaluate Eq. (1). Since the integrator setting is proportional to k_0, at least over the small ranges shown in Fig. 5, we determine the energy calibration by fitting the calculated yield curves to the data. Since the magnitude of the cross section is not known, we must allow for arbitrary normalization. This amounts to making a two-parameter least-squares fit of Eq. (1) to the data.

We recalculated the energy calibration using, instead of $\sigma(k)=$constant, the energy dependence of $\sigma(k)$ given by a preliminary experiment.[1] The calibrations from these two assumptions were equal within 100 kev. The best fit curves of the second assumption are shown in Fig. 5. The two calibration points have statistical accu-

[4] J. S. Pruitt and Steve R. Domen (unpublished results, 1958).
[5] Leiss, Pruitt, and Schrack (unpublished results, 1958).
[6] A. S. Penfold and J. E. Leiss, University of Illinois Report, 1958 (unpublished).

racy of $\frac{1}{2}\%$. Including possible errors arising from uncertainty in the energy dependence of the cross section, shape of the bremsstrahlung spectrum, calculation of the efficiency function, and other effects, the over-all accuracy of this calibration is about $\pm 1\%$.

In Fig. 6 we plot the calibration points obtained. Calibration of the machine energy at higher energies by this method becomes increasingly difficult because of the rapid decrease of the cross section with increasing energy. Also shown are a point at higher energy based on the π^0 meson threshold in C^{12} and a point at zero energy based on a pulser calibration of the integrator circuit.

GROUND-STATE CROSS SECTION

From the preceding discussion, we see that the yield curve measurements determine the ground-state cross section in addition to the energy calibration. They also show that the partial cross section to the first excited state of B^{11} (at 2.14 Mev) is much smaller than the ground-state cross section.

In order to determine the amount of first-excited-state cross section, the data shown in Fig. 5 were fitted by the sum of a ground-state yield curve and a first-excited-state yield curve with arbitrary coefficients. The ratio of first-excited-state to ground-state cross sections implied by these fits were 0.07 ± 0.19 for the 1-foil data and 0.10 ± 0.29 for the 7-foil data. Since this ratio depends on the details of the efficiency function, the same calculation was made for a preliminary experiment in which the efficiency function was considerably different from the present one. For those data the ratio was 0.00 ± 0.61, at about the same energy as the present 7-foil data. Combining these three measurements, the average first excited state cross section is 0.07 ± 0.16 times the ground-state cross section.

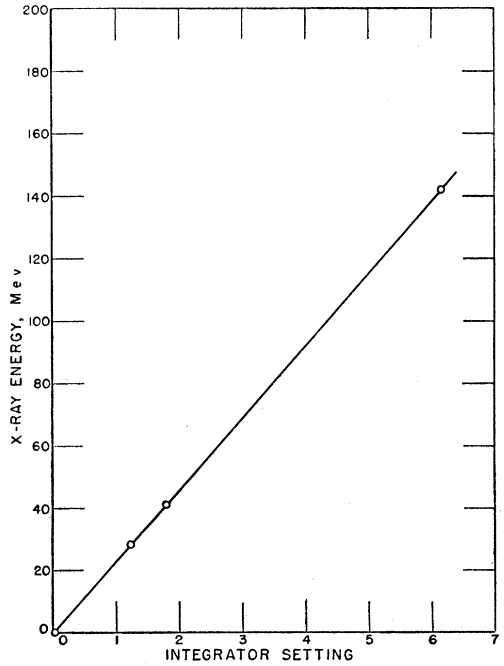

FIG. 6. Synchrotron energy calibration. The point near 140 Mev is obtained from the $C^{12}(\gamma,\pi^0)C^{12}$ reaction. The point at zero energy is a pulser calibration. The intermediate points are from the present experiment. Uncertainty of each measurement is smaller than the size of the circles shown.

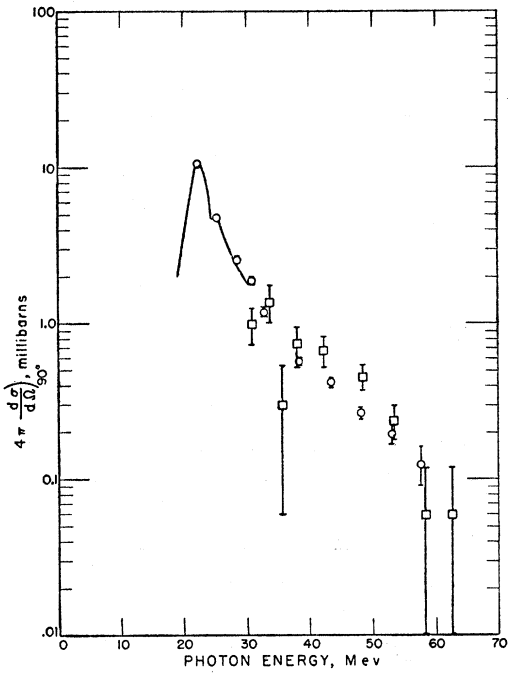

FIG. 7. $C^{12}(\gamma,p)B^{11}$ cross section at 90° as a function of photon energy. Circles are for the ground state and squares are for the low-lying excited states (assumed to be 5.03-Mev state). Uncertainties shown are statistical only. The solid curve is the 75° cross section obtained from the data of Barber[7] normalized to our data at 22.1 Mev.

Having obtained an energy calibration, and assuming that the partial cross section to the first excited state is zero, we may obtain the ground-state cross section at any energy by measuring one point on the yield curve with an appropriate absorber in front of the detector. In each case we assign the measurement to an appropriate mean energy, so that the result is nearly independent of the energy dependence of the cross section assumed for the purpose of calculating Eq. (1). The 90° cross sections obtained are shown in Fig. 7.

The ground-state cross sections are quite insensitive to the assumption that the first excited state cross section is negligible. If the first-excited-state cross section is $(7\pm16)\%$ as large as the ground state, as estimated above, the calculated ground-state cross sections are then about $(4\pm8)\%$ too high.

The error in our calculated cross sections due to assuming an incorrect energy dependence depends primarily on the second derivative of the cross section with energy evaluated at the mean energy. The effect is

TABLE II. Ground-state cross sections. Differential cross sections are given in millibarns per steradian, the total cross sections in millibarns.

Angle (deg) \ Photon energy (Mev)	22.1	25.3	30.7	38.2	48.2
30	0.47±0.03	0.25±0.02	...	0.054±0.005	...
37.5	0.52±0.03	0.33±0.03	0.115±0.012	0.066±0.006	0.046±0.006
45	0.62±0.03	0.31±0.03	0.120±0.012	0.069±0.006	0.052±0.007
60	0.72±0.04	0.43±0.03	0.166±0.014	0.075±0.006	0.051±0.007
75	0.82±0.04	0.41±0.03	0.178±0.015	0.078±0.006	0.036±0.005
90	0.83±0.03	0.38±0.01	0.149±0.008	0.045±0.003	0.021±0.002
105	0.80±0.04	0.32±0.02	0.111±0.011	0.040±0.005	0.008±0.004
120	0.64±0.04	0.34±0.03	0.077±0.010	0.024±0.004	0.004±0.004
135	0.49±0.03	0.20±0.02	0.065±0.010	0.012±0.003	0.006±0.004
142.5	0.46±0.03	0.16±0.02	0.041±0.008	0.010±0.003	0.008±0.005
150	0.37±0.03	0.15±0.02	0.030±0.007	0.008±0.003	0.000±0.007
Total cross section	8.13±0.13	3.86±0.08	1.38 ±0.05	0.54 ±0.02	0.30 ±0.02

negligible except at our lowest energy point which is near the peak of the giant resonance. In calculating this point, we assumed the energy dependence measured by Barber.[7] We obtain the same result assuming for the energy dependence a smooth curve through the data of Cohen *et al.*[8] The assumed shapes both have a giant resonance full width at half-maximum of about 3.6 Mev. Our calculated cross section at 22.1 Mev photon energy is inversely proportional to the assumed width of the giant resonance.

To attempt to account for the above and other systematic uncertainties, we have assigned an uncertainty of 30% in addition to statistical uncertainties to the measurement at 22.1 Mev, and a corresponding 15% uncertainty to all other points.

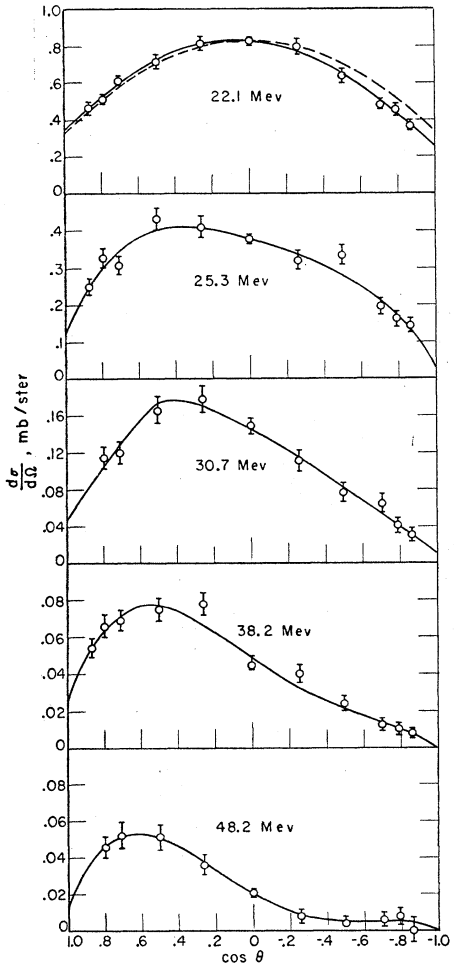

FIG. 8. Ground-state angular distributions at five photon energies. The solid curves are least-squares fits (see text). The dashed curve with the 22.1-Mev data is proportional to $2+3\sin^2\theta$, normalized to our data at 90°. The curves are labelled with the appropriate photon energy. Note that the cross-section scales are not all equal. Uncertainties shown are statistical only.

ANGULAR DISTRIBUTIONS

The cross section as a function of angle is proportional to the measured yield as a function of angle except for easily calculated geometrical factors. The difference between laboratory system and center-of-momentum system is negligible for this reaction in the energy region studied. The five measured ground-state angular distributions are shown in Fig. 8 and listed in Table II. A small correction has been made for the finite angular interval covered by the detector by assuming that the measured angular distribution is approximately correct and performing a first order iteration. This correction was usually about 1% and was never more than 9%. The angular distributions obtained were fitted by

$$\frac{d\sigma}{d\Omega}(\theta)=\sum_{i=0}^{4} a_i \cos^i\theta, \qquad (2)$$

where θ is the angle between the x-ray beam and the proton detector, using the least-squares method. The calculations were done on the National Bureau of Standards IBM 704 computer. The best fits are shown in Fig. 8. The coefficients $a_0, \cdots, a_4$ of the angular distribution are listed in Table III together with the

[7] W. C. Barber (private communication).
[8] Cohen, Mann, Patton, Reibel, Stephens, and Winhold, Phys. Rev. **104**, 108 (1956).

TABLE III. Angular distribution coefficients.

Photon energy, Mev		22.1	25.3	30.7	38.2	48.2
Coefficients of power series fit, Eq. (2)	a_0	0.832±0.021	0.380±0.012	0.148±0.007	0.0490±0.0023	0.0208±0.0016
	a_1	0.085±0.056	0.145±0.041	0.112±0.022	0.0702±0.0077	0.0587±0.096
	a_2	−0.590±0.142	−0.100±0.095	−0.081±0.051	0.0134±0.0161	0.0442±0.0202
	a_3	−0.039±0.087	−0.101±0.064	−0.114±0.040	−0.0575±0.0120	−0.0518±0.0179
	a_4	0.059±0.179	−0.199±0.125	−0.056±0.073	−0.0510±0.0211	−0.0577±0.0327
Coefficients of Legendre polynomial fit, Eq. (3)	c_0	0.647±0.010	0.307±0.007	0.110±0.004	0.0433±0.0013	0.0240±0.0016
	c_1	0.061±0.015	0.084±0.011	0.044±0.007	0.0356±0.0020	0.0276±0.0035
	c_2	−0.360±0.025	−0.181±0.018	−0.086±0.013	0.0202±0.0033	0.0035±0.0067
	c_3	−0.016±0.035	−0.041±0.026	−0.045±0.016	−0.0230±0.0048	−0.0207±0.0072
	c_4	0.013±0.041	−0.046±0.029	−0.013±0.017	−0.0117±0.0048	−0.0132±0.0075

coefficients of the function

$$\frac{d\sigma}{d\Omega}(\theta)=\sum_{l=0}^{4} c_l P_l(\cos\theta), \tag{3}$$

where P_l are the Legendre polynomials, normalized such that

$$\int_{-1}^{1} P_l^2(x)dx=\frac{2}{(2l+1)}. \tag{4}$$

The coefficients of the Legendre polynomials are plotted as a function of incident photon energy in Fig. 9. Note that $4\pi c_0$ is the total cross section.

EXCITED STATE CROSS SECTIONS

The proton yield curves shown in Fig. 5 were extended to higher photon energies in an attempt to measure partial cross sections for leaving the residual nucleus in excited states.[9] The data are shown in Fig. 10. It can be seen that the calculated ground-state yield which is an excellent fit to the data for the first six Mev above threshold does not account for all the yield at higher energies. The excess yield must be due to transitions in which the residual nucleus is left in excited states. In particular, if we assume that all of the yield not due to the ground state is due to the excited state at 5.03 Mev, we obtain the calculated yield curves shown in Fig. 10. This is the best fit that we can make by assuming only one excited state contributes, although a fairly good fit can also be made using the 4.46-Mev state instead of the one at 5.03 Mev.

The magnitudes of 5.03-Mev state yield curves needed to obtain the agreement shown in Fig. 10 are used to calculate the partial cross sections to this state. Within the limits of resolution and precision of the experiment, we can only say that the cross section so calculated is approximately the sum of the partial cross sections for the low-lying excited states of B^{11}.

For absorbers other than those of Fig. 10, we obtain the excited-state cross section at 90° from a yield measurement at just one bremsstrahlung energy (~10 Mev above ground state threshold), in addition to the measurement which gives the ground-state cross section.

The accuracy of the excited-state cross section measurement is not very good, largely because of the propagation of errors in the ground-state measurements and in the calculations. For this reason, the excited-state data for absorber number 0 was discarded as useless. The values quoted in Table IV should be reliable to about ±50% in addition to the quoted counting statistics and are to be interpreted as the sum of partial cross sections for the low-lying excited states, with major contributions from the 4.46-Mev or 5.03-Mev state, or both. The results are plotted in Fig. 7.

Although our proton yields can contain contributions from the (γ,pn) process, measurements of ground-state and low-lying excited state cross sections are not affected because the (γ,pn) threshold is 11.5 Mev above

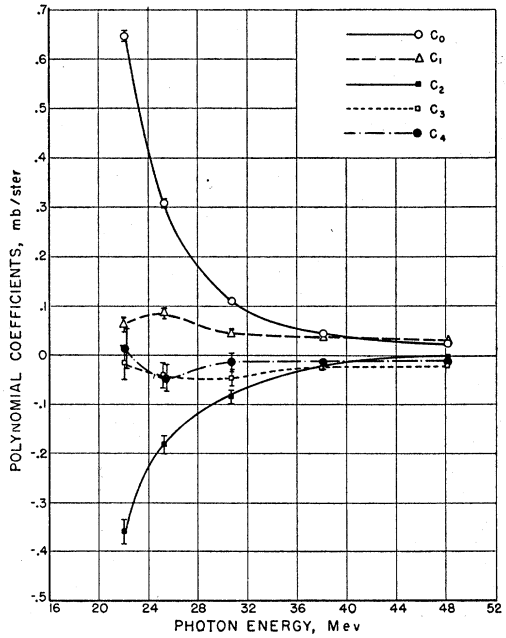

FIG. 9. Coefficients (c_l) of Legendre polynomials (P_l) for the least-squares fits shown in Fig. 8 as a function of energy. Uncertainties shown are statistical only. Where no uncertainty is shown, it is smaller than the size of the symbol. The smooth curves are for illustrative purposes only.

[9] We assume the B^{11} level scheme given by F. Ajzenberg and T. Lauritsen, Revs. Modern Phys. **24**, 321 (1952).

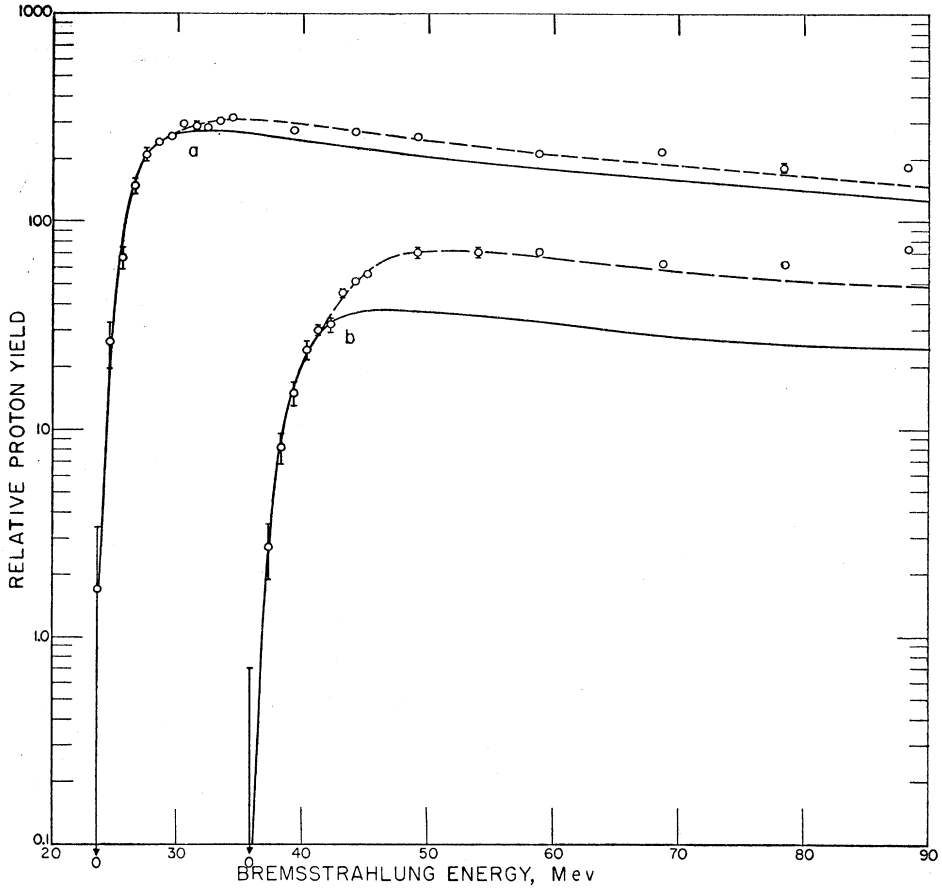

FIG. 10. Proton yield at 90° as a function of photon energy. The uncertainties shown are statistical only. The solid curves are the best fits to the ground-state yields determined from the six points at lowest energies. The dashed curves include excited state contributions assumed to be from the B^{11} state at 5.03 Mev. The excess at higher energies is probably due to the $C^{12}(\gamma,pn)B^{10}$ reaction.[10] (a) Data for absorber number one. (b) Data for absorber number seven.

the (γ,p) threshold. It is quite likely, however, that some of the difference between observed yield and calculated yield in the 60- to 90-Mev region is due to this process. The measurements of Smith[10] indicate that the (γ,pn) "pseudodeuteron" process does occur in this energy range with approximately the energy dependence seen here.

Angular distributions were measured, using absorber number seven, at 58.9- and 88.3-Mev bremsstrahlung energy in addition to the measurement at 41.3 Mev which determined the ground state angular distribution. The fact that the angular distribution at the higher energies is very different from that measured at 41.3 Mev confirms the conclusion that the proton yields at higher energies contain important contributions from excited-state transitions.

By subtracting from the measured data at 58.9-Mev bremsstrahlung energy the ground-state angular distribution, renormalized by the ratio of calculated ground-state yields at 58.9 and 41.3 Mev, we obtain the angular distribution for the excited-state transitions. The result is shown in Fig. 11. Although the accuracy is poor, this angular distribution is very different from the ground-state angular distributions in the same energy range. The angular distribution at 88.3 Mev is very similar to the one at 58.9 Mev.

TABLE IV. Excited state cross section at 90°.[a]

Photon energy, Mev	$4\pi(d\sigma/d\Omega)_{90°}$ millibarns
30.9	1.0 ±0.3
33.6	1.4 ±0.4
35.8	0.3 ±0.2
38.0	0.8 ±0.2
42.2	0.7 ±0.2
48.5	0.5 ±0.1
53.3	0.2 ±0.1
58.3	0.06±0.06
62.7	0.06±0.06

[a] A 50% uncertainty in addition to the statistical uncertainty indicated is present in these results.

CONCLUSIONS

The $C^{12}(\gamma,p)B^{11}$ partial cross section to the ground state of B^{11} has been measured over a wide range of energy and angle. The results show a high-energy "tail" above the giant resonance which extends to photon energies of at least 58 Mev. The angular distribution near the peak of the giant resonance (22.1 Mev) is rather similar to the $2+3\sin^2\theta$ distribution predicted

[10] J. H. Smith and S. I. Baker, Bull. Am. Phys. Soc. Ser. II, 3, 172 (1958).

for the dipole resonance by the single particle model.[11] The observed deviation from this prediction is significant even near the peak of the resonance. This demonstrates the importance of non-electric-dipole contributions to the cross section. The relative importance of the nondipole part increases rapidly with increasing energy, as shown by the increasing asymmetry of the angular distribution.

The total cross section to the ground state at 22.1 Mev, near the peak of the giant resonance, is 8.13 mb, somewhat lower than previously reported results.[7,8] The accuracy of the present measurement at this energy, however, is rather poor (~30%), largely because of the sensitivity of the result at this energy to the detailed shape of the proton resolution function, so that we do not regard the disagreement as being serious. The uncertainty in our measurements at all higher energies is much smaller (~15%).

The ground-state cross section which has been measured involves initial and final states which are completely specified. (The spins and parities of C^{12} and B^{11} are known.) It should therefore be possible to calculate the cross section with a minimum of approximations. This experiment should thus be a sensitive test of theory. For example, in a shell-model calculation, the wave functions would have to be quite accurate in order to provide a good fit to the data over the entire energy range.

The cross section to the first excited state of B^{11} is found to be much smaller than the ground-state cross section. This may be partly understood on the basis of intermediate coupling. If one decomposes the 8-nucleon p-shell configuration of C^{12} as given by Kurath[12] into sums of products of 7-nucleon terms and one-nucleon terms, the major contributions are from configurations in which the 7-nucleon "parent" has angular momentum $J=\frac{3}{2}$. There is a smaller contribution from parent states with $J=\frac{1}{2}$, and no other appreciable terms. Neglecting second order effects, the cross section must then involve B^{11} states which are parents of the C^{12} configuration. Thus, the largest partial cross sections will involve $J=\frac{3}{2}$ states of B^{11} (as the ground state), with smaller contributions from $J=\frac{1}{2}$ states (as the first excited state).

[11] G. R. Bishop and R. Wilson, in *Encyclopedia of Physics* (Springer-Verlag, Berlin, 1957), Vol. 42, p. 341.
[12] Dieter Kurath, Phys. Rev. **101**, 216 (1956).

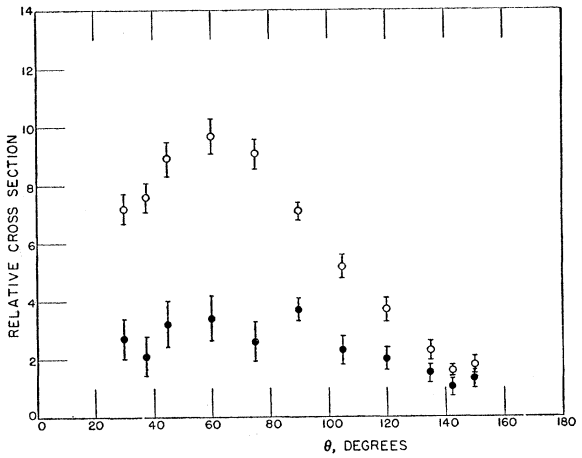

FIG. 11. Angular distribution at 58.9-Mev bremsstrahlung energy using absorber number seven. The open circles are measured values. The solid circles are obtained by subtracting the ground-state contribution. Uncertainties shown are statistical only.

If the above analysis is correct, then our data would seem to indicate that at least one of the states of B^{11}, at 4.46 or 5.03 Mev, has $J=\frac{3}{2}$, because the cross section to the low-lying excited states is shown to be comparable with the ground-state cross section above 30-Mev photon energy. (These states would not contribute appreciably near the peak of the giant resonance because the thresholds are too high.)

A method for calibrating the energy scale of an electron accelerator has been developed. The method provides calibrations with an accuracy of better than one percent in an energy region where convenient reaction thresholds are not available as calibration points. The agreement of this calibration with previous calibrations of our synchrotron energy scale proves that it is indeed the cross section to the ground state of B^{11}, rather than some excited state, which has been observed.

ACKNOWLEDGMENTS

The authors wish to thank M. Danos and P. De Celles for many interesting discussions of the theoretical interpretations of these results. The aid of P. Walsh in making least-squares calculations with the digital computer is also gratefully acknowledged.